

NaCo/SAM observations of sources at the Galactic Center

J. Sanchez-Bermudez¹, R. Schödel¹, A. Alberdi¹, J. U. Pott²

¹ Instituto de Astrofísica de Andalucía (CSIC), C/ Glorieta de la Astronomía S/N, 18008 Granada, Spain

² I. Physikalisches Institut, University of Cologne, Zùlpicher Str. 77, 50937 Köln, Germany

E-mail: joel@iaa.es, rainer@iaa.es, antxon@iaa.es, pott@ph1.uni-koeln.de

Abstract. Sparse aperture masking (SAM) interferometry combined with Adaptive Optics (AO) is a technique that is uniquely suited to investigate structures near the diffraction limit of large telescopes. The strengths of the technique are a robust calibration of the Point Spread Function (PSF) while maintaining a relatively high dynamic range. We used SAM+AO observations to investigate the circumstellar environment of several bright sources with infrared excess in the central parsec of the Galaxy. For our observations, unstable atmospheric conditions as well as significant residuals after the background subtraction presented serious problems for the standard approach of calibrating SAM data via interspersed observations of reference stars. We circumvented these difficulties by constructing a synthesized calibrator directly from sources within the field-of-view. When observing crowded fields, this novel method can boost the efficiency of SAM observations because it renders interspersed calibrator observations unnecessary. Here, we presented the first NaCo/SAM images reconstructed using this method.

1. Introductory Remarks

The Galactic center (GC) nuclear stellar cluster (NSC), the densest region of the Milky Way ($\rho > 10^6 M_{\odot} \text{ pc}^{-3}$) [1; 2], contains the supermassive black hole (BH) SagittariusA* (SgrA*) at its center [3; 4] and exhibits signs of at least two epochs of recent star formation [5; 6]. Theoretical considerations as well as observational evidence suggest that the GC environment favors a top-heavy initial mass function (IMF) [7–9] (see however Do et al., these proceedings). On the order of 100 high-mass stars were created in the most recent ($\approx 4 \times 10^6$ years-old) starburst episode in the central parsec of the GC. Since massive stars are rare in the Galaxy, this makes the Milky Way NSC an important site to study the properties of such objects (e.g. morphology, multiplicity) and their interactions with the interstellar medium (ISM).

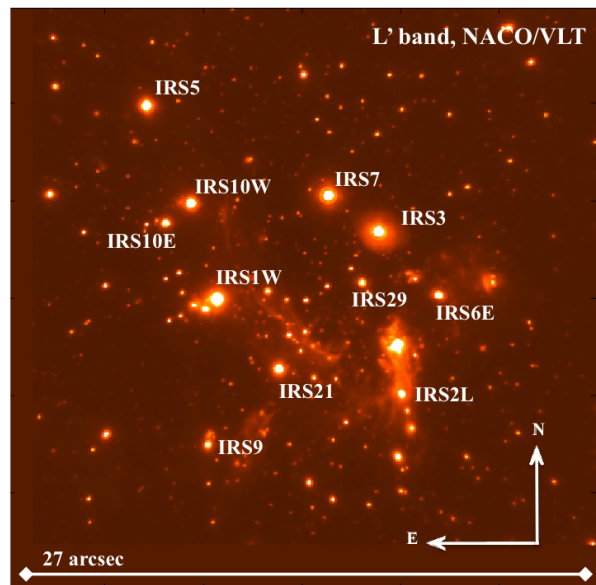


Figure 1: The inner central parsec of the GC in the L'-band with NaCo/VLT. Our targets, the brighter massive stars in the field with known diffuse (resolved and/or unresolved) emission, are identified by their names.

Figure 1 provides an overview of the central parsec of the Galaxy in the form of an L'-band AO image obtained with the NaCo instrument of the Very Large Telescope (VLT). Our targets, the brighter sources ($4 < \text{mag}_L < 7$) in the field of view (FOV), are labeled with their names. The principal selection criteria for this sample are that all of the sources (a) exhibit significant mid-infrared excess, (b) are related to recent starburst events (~ 6 and ~ 100 Myr ago) and (c) show extended structure like dusty outflows and bow-shocks. Our sources can be divided into three main groups: (a) **Evolved (super-) giants**, like IRS 7, 9, 3; (b) **Massive, post-main sequence stars**, such as IRS 6E, 29NE1 and (c) **Bow-shocks**, as IRS 1W, 21, 10W, and 5.

The importance of a detailed study of such objects with high angular resolution lies in the possibility to understand the role of binarity/multiplicity in the dust formation processes, as well as the circumstellar dust distribution. In this context, Sparse Aperture Masking interferometry + Adaptive Optics is one of the most suitable techniques to address these goals. Nevertheless, because of the difficulties we encountered during the observations (bad atmospheric conditions, difficulty of measuring the sky emission), the analysis of our SAM data requires the development of dedicated software and new reduction techniques to boost the efficiency of the observations. In this work, we present a novel calibration technique, as well as our first reconstructed SAM images of the targets described above.

2. Brief description of the technique

Adaptive Optics (AO) is a powerful technique which is used to overcome the degrading effects (mainly induced by the atmospheric turbulence) in the wavefront (WF) of a specific source, while keeping high sensitivity. Nevertheless, in spite of the great promise of this technique to provide us with diffraction limited images, it still faces a number of problems that make a precise and stable PSF calibration very difficult. Such problems are, for example: (a) The PSF of the AO systems is variable on different timescales and highly sensitive to the observing conditions (e.g. seeing, airmass, etc); (b) the AO performance is constrained by technological limitations of the system (e.g. the number of sensors and actuators that measure and correct the incoming WF); and (c) the WF of the guide star is not the same as the one of the science objects. Therefore, their wavefronts suffer different distortions because they take slightly different paths through the atmosphere (anisoplanatism) [10; 11].

Sparse Aperture Masking (SAM) interferometry is a technique which transforms a single dish telescope into a non-redundant Fizeau interferometer by placing a mask with many holes in the pupil plane of the telescope camera. The main advantage of SAM interferometry is the fact that the non-redundant mask (NRM) removes most of the incoherent noise produced by the atmospheric turbulence. In this way, a very well defined and stable PSF can be obtained. The PSF resembles the diffraction pattern of the mask (see Fig. 2). The nominal angular resolution (θ , which corresponds to the Full-Width Half-Maximum of the beam) achieved by this technique is of the order of $\theta \approx \lambda/2D$. This is a factor of ~ 2 better than the resolution obtained in standard imaging. Nevertheless, due to the fact that the NRM covers most of the telescope pupil, SAM suffers from low photon efficiency and is limited to bright objects (e.g. in the case of the VLT the magnitudes of the targets range between 4 to 12, depending on the mask used). **A combination of the technologies of SAM and AO offers us a unique tool to recover high fidelity images and, hence, study structures between one and few times the PSF size (e.g. in the case of the VLT, to analyze morphologies in the regime of 50 to 150 mas), with the strengths of the robust PSF calibration provided by SAM, and the higher dynamic range obtained by the AO systems [11].**

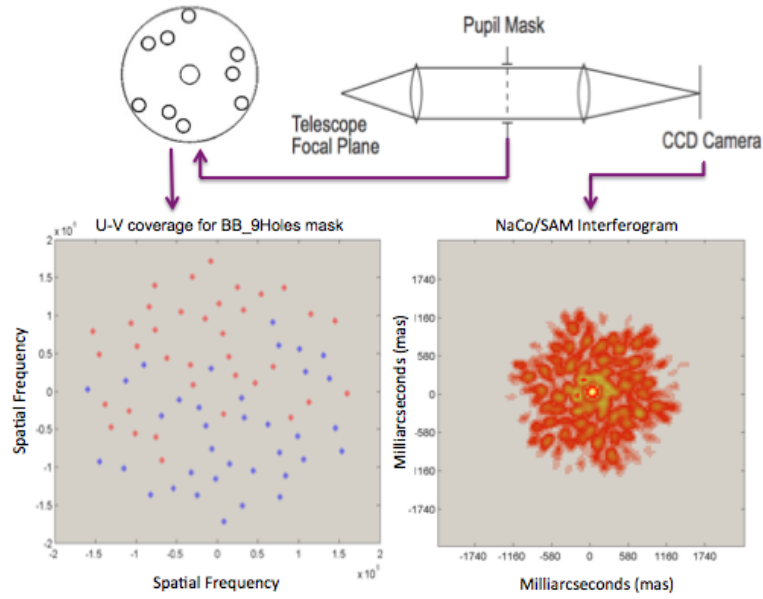


Figure 2: Sparse Aperture Masking layout. In the figure a NRM with nine holes is located in the pupil of the telescope. It is thus transformed into an interferometer with a non-redundant u-v coverage (lower-left gray scheme); note that the number of points sampled in the Fourier space correspond to all baselines formed by all the possible pair of holes combinations plus their complex conjugates (in this case, 36 red dots + 36 blue dots). The lower-right gray scheme shows the SAM interferogram (i. e. interferogram) of a PSF obtained at the camera detector, with a shape that only depends on the geometry of the interferometric array. The upper part of the scheme was adapted from the NaCo manual and Tuthill et al. (2006).

3. NaCo/SAM L-band observations of the Galactic Center

3.1. NaCo/SAM observational setup

In June 2010 we performed VLT NaCo/SAM observations of the central parsec of the GC NSC in the L band, using two different filters; (i) L' ($3.8 \mu\text{m}$) and (ii) NB 3.74 ($3.74 \mu\text{m}$). The observations in the L' filter were conducted using the *BB_9holes* mask, while the ones in the NB 3.74 filter were taken using the *9_holes* mask. The main reason to use these NRMs is because they are optimized to be utilized with broad band and narrow band filters, respectively. The observations were recorded using the Pupil-Tracking mode of NaCo (which freezes the pupil and makes the FOV rotate in opposite direction to the parallactic angle). The so-called *cube mode* was used, which saves each single data integration time (DIT) frame. The advantage of the cube mode is that it allows the selection of the best frames. Frame selection can become necessary when AO performance is not stable, as it was the case for the observations described here. Our observations consisted of a group of 13 sets of data-cubes composed of 20 - 30 exposures with 5 sec of DIT. Because SAM removes the low spatial frequencies related to the atmospheric noise,

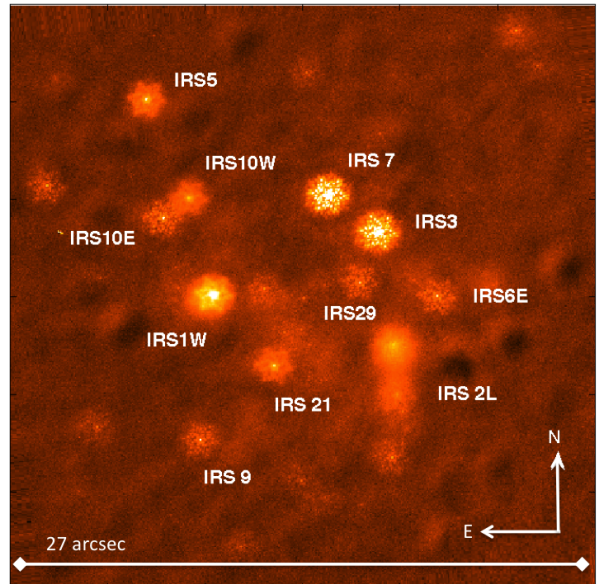


Figure 3: NaCo/SAM FOV. The main targets of our sample show clearly the interference pattern of the NRM overimposed on them and are labeled with their names. Since SAM is a Fizeau type interferometry, it keeps the entire FOV of the camera used.

chopping techniques were not used to eliminate the near-infrared background radiation. Nevertheless, since the GC NSC is extremely crowded, separate sky observations were taken on a dark cloud a few arcmin to the north-west of Sgra*. IRS7, the brightest target in our FOV, was used as guide star for the the IR WFS of NaCo. Figure 3 shows a single Naco/SAM exposure with our targets identified on it.

3.2. Data Reduction

The reduction process of our NaCo/SAM data-cubes is divided into two principal steps: (i) standard imaging reduction and (ii) interferometric analysis.

3.2.1. Standard Imaging: In this reduction part, as in any other optical-NIR imaging observations, all data-cubes were flat-fielded, bad-pixel corrected and background subtracted. Depending on the observational data set, the sky template for the background subtraction was obtained by calculating either (i) the median of the sky cubes or (ii) through the median of the lower values at each pixel from the dithered images, when no dedicated sky observations close in time were available. As our images were taken using the Pupil Tracking mode of NaCo, all cubes had to be derotated to correctly compute the interferometric observables. All data-cubes were frame selected, discarding bad images through the analysis of the cube flux statistics (~ 70 - 90 % of the frames were eliminated). Finally, each one of the individual targets was stored into a subcube of 128×128 pixels.

3.2.2. Interferometric reduction process: To obtain the interferometric observables (squared visibilities and closure phases) we used Michael Ireland’s IDL pipeline. This code calculates the Fourier transform of all the frames in a given data-cube and convolve them with a *matched filter* template, which is the Fourier transform of all baselines formed by the holes in the NRM. Due to the facts that (i) each hole in the NRM has a finite radius, and (ii) that our data cubes are stored into a discrete array of pixels, the normalized flux at every baseline in the Fourier space is spread into a group of pixels, or **splodge**, around the central spatial frequency of the used baseline (see Fig 4). Therefore, every raw (not calibrated) squared visibility is calculated by the squared value of the sum of the normalized flux at a given splodge, divided by the total flux received (i.e. baseline zero). The closure phases are the arguments of the bispectra, i.e. the ensemble of all visibility products for non-redundant baseline triangles. It is important to remark that: the visibility amplitudes give us information about the compactness and extension of the source brightness distribution in all the spatial frequencies sampled by the baselines of our interferometer, while closure phases contains information on the orientation and symmetry of the target structure and are robust to any observational effect (e.g. atmospheric turbulence).

In order to increase the u-v coverage and to get a better sampling of the sources brightness distribution (see Fig. 5) we use the Earth rotation synthesis through the combination of the visibilities obtained by observations of the targets at different parallactic angles. An example of the IRS7 raw visibilities and closure phases is shown in Figure 6.

3.2.3. Calibration of visibilities and closure phases. The standard observing technique for NaCo/SAM is the observation of a science target interwoven with observations of a nearby point-source reference object (i.e. the calibrator). This star should be observed at similar airmass and in the same AO configuration as the science target. Therefore, calibrator sources should be of similar brightness as the targets. Unfortunately, this was not possible for our observations because of the following difficulties:

(a) Rapidly changing observing conditions (clouds, highly variable seeing, etc.) affected the calibrator observations, so that it was hard to obtain data of similar quality on source and calibrators;

(b) The GC is highly extinguished. Hence, it is very difficult to find calibrators that are sufficiently bright in the L band ($\sim 4 \text{ mag}_L$) because the ones that fulfill this condition are too bright in the K-band so that they would saturate the infrared wavefront sensor of NaCo. Therefore, the observed calibrators were systematically fainter than our brighter targets (e.g. IRS7 and IRS 3);

(c) The observations were affected by strong residual patterns that remained in the images after background subtraction. The reason for these residuals are not clear, but they are typical for L-band observations, where the background fluctuates rapidly (see Fig. 7).

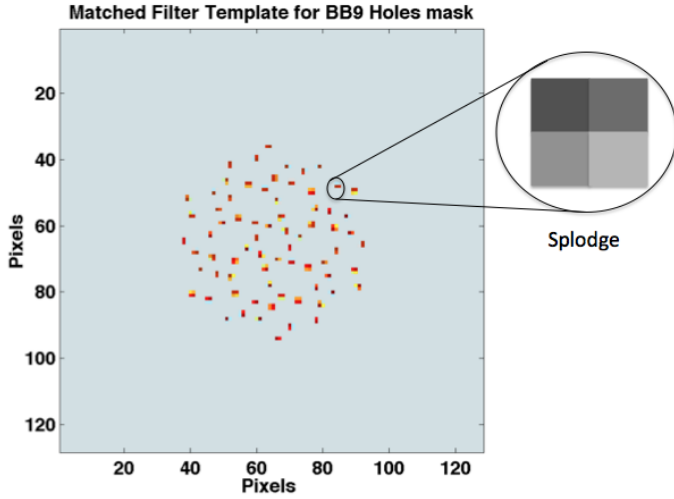


Figure 4: Matched Filter Template. The total flux at every spatial frequency (given by every baseline of the mask) sampled in the matched filter is spread in a series of pixels called “splodges”. The total amount of pixels which form a splodge is determined by the size of the mask holes.

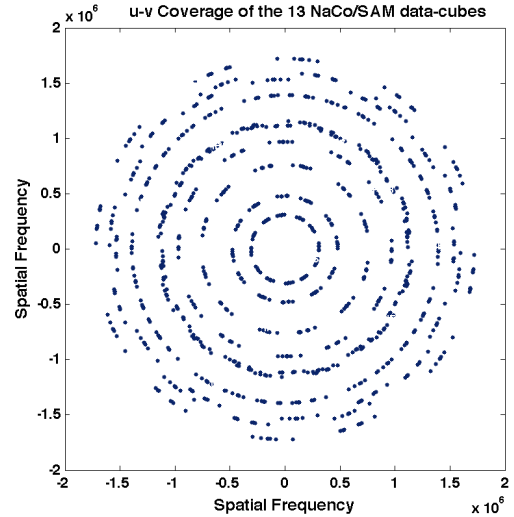


Figure 5: NaCo/SAM total u-v coverage. The total u-v coverage of our interferometer is produced using the Earth Rotation Synthesis through the combination of all data-cubes visibilities. The beam is symmetric in all directions.

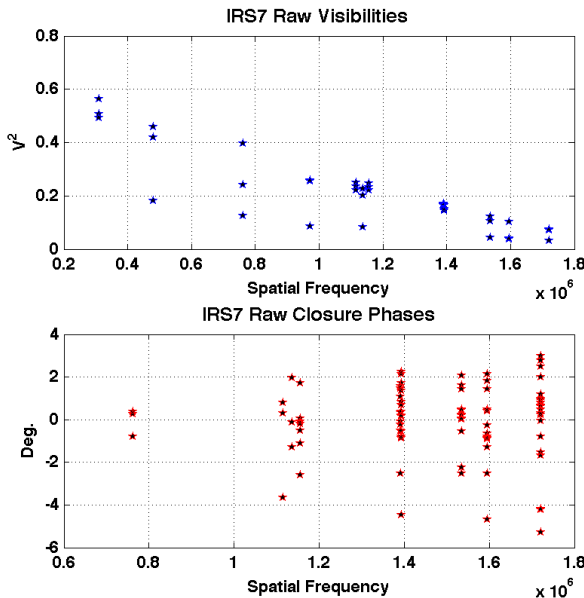


Figure 6: Raw Squared visibilities and Closure phases of IRS7. On the figure we have the uncalibrated 36 visibilities and 84 closure phases of one of the observed IRS7 L-band data-cubes using the *BB_9holes* mask.

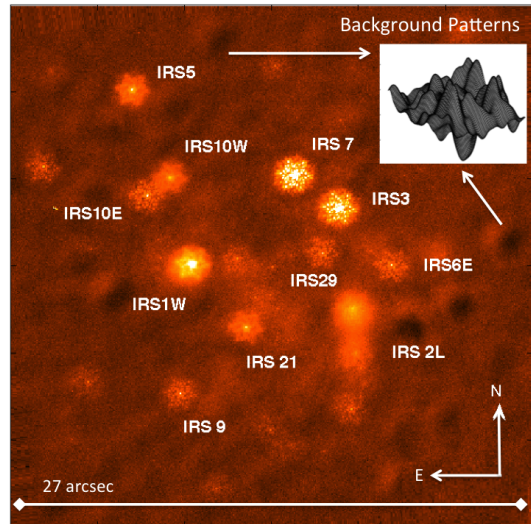


Figure 7: L-band NaCo/SAM background patterns. All frames of our observations exhibit some background patterns spread all over the FOV. The angular scale of the background variations is of the order of the size of the PSF ($\sim 1''$).

In order to overcome these problems we developed a calibration technique, which we called the “*Synthetic Calibrator*”. This method takes advantage of the presence of several bright sources in our FOV and creates a PSF by source superposition, using StarFinder [12] routines. The images of stars are extracted from the FOV, cleaned from the contamination of secondary sources, locally background subtracted, centered with sub-pixel accuracy, normalized and combined by a median superposition. The resulting PSF is thus obtained directly from the field, without the need to observe a calibrator source. Some of the advantages are: (a) No interwoven observations of standard calibrators are needed, therefore, the observing conditions are exactly the same for both the calibrator and the target; (b) the calibrators can be as bright as science targets.

Note that, a priori, we do not know the intrinsic source-structure of our targets. This can be a source of systematic uncertainties when extracting a synthetic calibrator. Nevertheless, the latter effect, as well as the background residuals, are effectively minimized by the median superposition of several sources when creating the synthetic calibrator, as our tests have confirmed. Figure 8 shows an example of the calibrated visibilities and closure phases of two of our targets IRS 7 and IRS 1W obtained with this technique. Of course, the Synthetic Calibrator technique can only be used when several sufficiently bright sources are present within the field-of-view. It may thus be ideal for observations of stars in dense clusters.

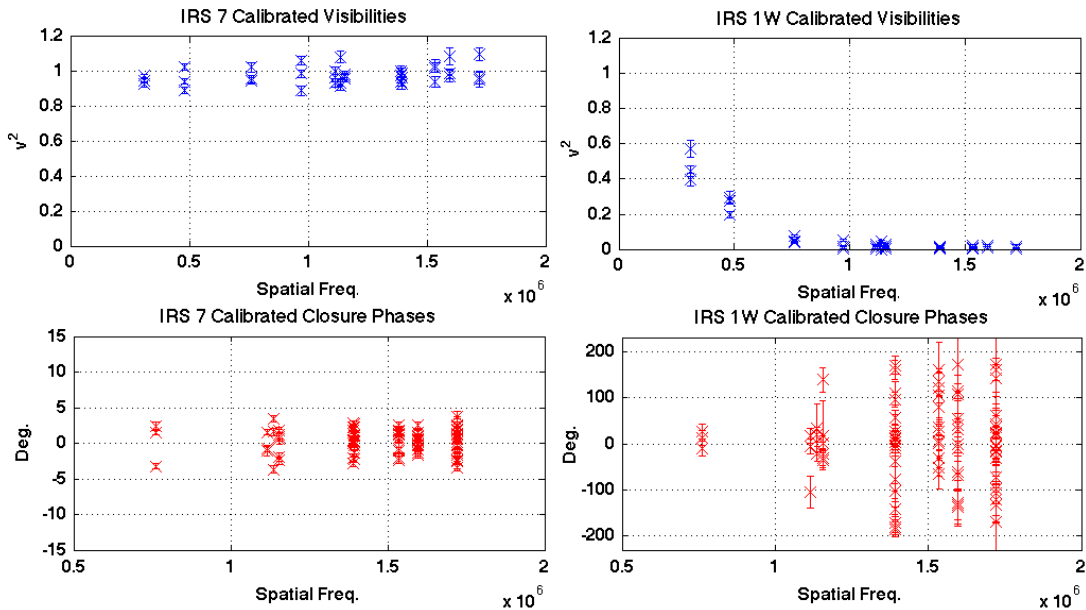


Figure 8: Calibrated Visibilities and Closure Phases of IRS 7 and IRS 1W. Calibrated visibilities of IRS 7 are constant and close to the unit, demonstrating that this source is a point-like object; its closure phases also confirm the point-symmetry of the object (left). On the other hand, the visibilities of IRS 1W suggest the existence of an extended structure larger than the interferometric beam; its closure phases demonstrate the point asymmetry of this source (right).

4. Image reconstruction.

Once the calibrated interferometric observables had been obtained, image reconstruction was done with the BSMEM package [13], which uses a maximum entropy algorithm to reconstruct the interferometric maps. Figure 9 displays a comparison between three of our reconstructed SAM images (IRS 1W, IRS 5 and IRS 10W) in the L-band (upper part) and the AO deconvolved Ks images of the same sources (lower part) obtained with the 10-meter Keck telescope by Tanner et al. (2005) [14]. The resolution achieved with our SAM observations in the L-band (at $3.8 \mu\text{m}$, $\theta \approx 60 \text{ mas}$) is similar to the one obtained by the AO system of Keck telescope in the Ks band (at $2.2 \mu\text{m}$, $\theta \approx 45 \text{ mas}$). This demonstrates that the nominal resolution of the NaCo/SAM technique has been achieved. On the other hand, Figure 10 presents for comparison a set of six L-band

images taken with the VLT. The first column shows our SAM images, the second one displays Lucy-Richardson [15] deconvolved images and the third one corresponds to raw AO images. The resolution and quality of the reconstructed SAM images surpass the raw and deconvolved AO images at the same frequency.

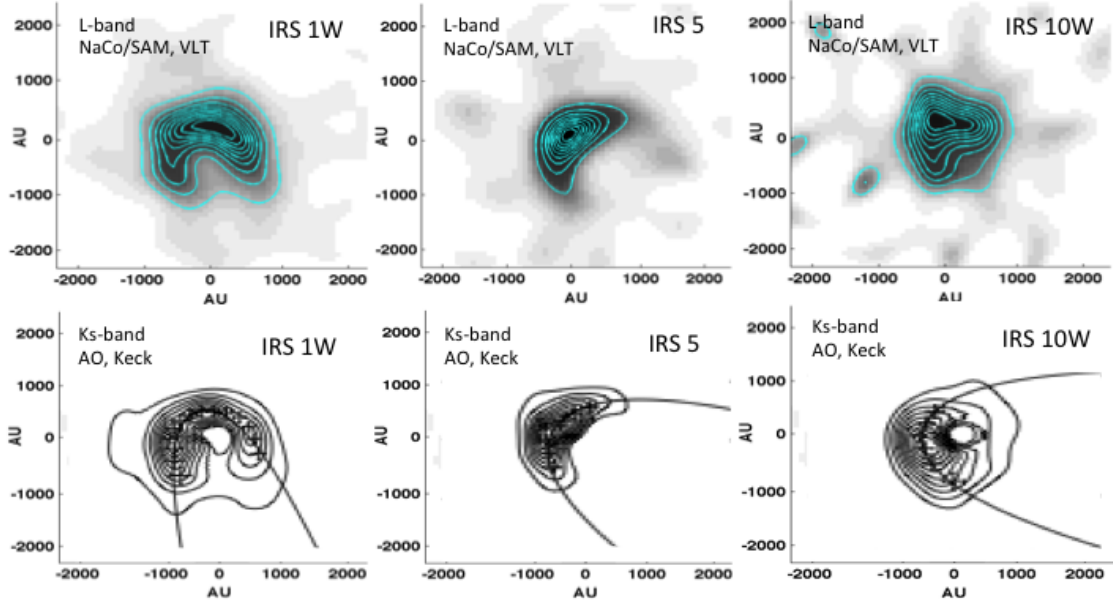


Figure 9: NaCo/SAM vs AO Keck images. At the top, NaCo/SAM images of IRS 1W, IRS 5 and IRS 10W in the L-band; in the bottom, the same sources are presented as deconvolved AO images in the K-band. The angular resolution of both subsets of images is similar, even though there is a difference in wavelength. The K-band images are adapted from Tanner et al (2005). Contours of NaCo/SAM images represent 10, 20, 30, 40, 50, 60, 70, 80 and 90 % of the total normalized flux.

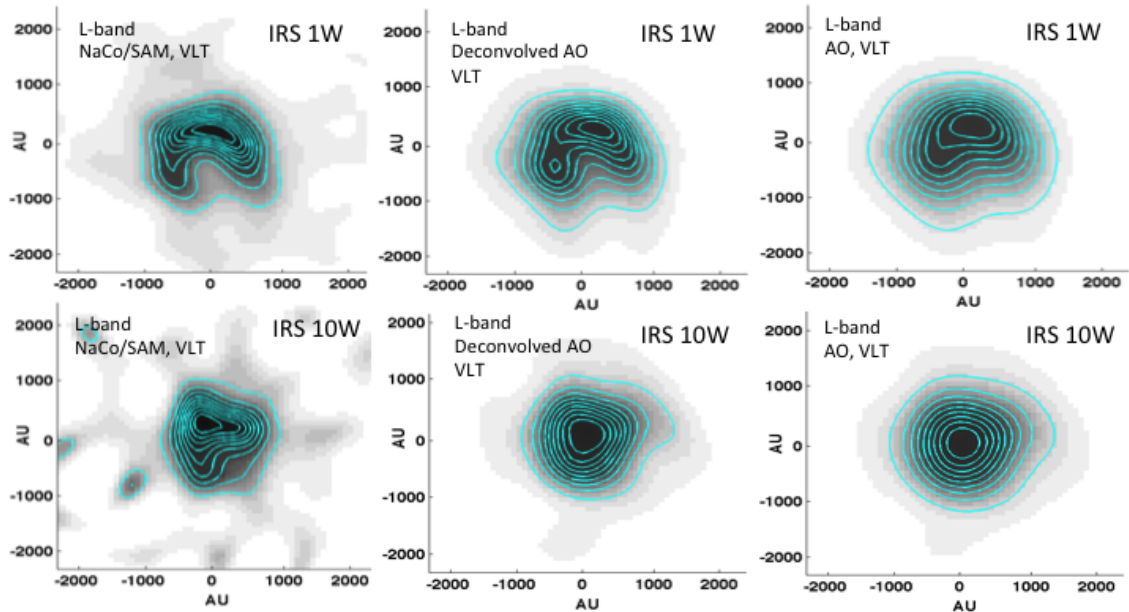


Figure 10: NaCo/SAM vs AO. IRS 1W and IRS 10W are presented in three subsets of images: at the left, in the form of NaCo/SAM images; in the middle, as Lucy-Richardson deconvolved images; to the right, as non-deconvolved AO images. Note how the resolution on the NaCo/SAM images surpasses the ones obtained by the other two subsets. Contours represent 10, 20, 30, 40, 50, 60, 70, 80 and 90 % of the total normalized flux.

5. Summary

We overcome the difficulties of our NaCo/SAM observations (highly variable weather conditions, background instabilities and calibration problems) with the creation of “*The Synthetic Calibrator*” from the median superposition of several sources in the field, which according to our results appears to be a promising new way to calibrate SAM observations of dense stellar fields. The strength of this technique relies on the opportunity to observe multiple targets at the same time in Stellar Clusters, thus increasing the efficiency of the observations by eliminating the necessity of interspersed observations between standard calibrators and targets. From our reconstructed NaCo/SAM images we can conclude that the nominal L-band NaCo/SAM resolution was achieved ($\theta \approx 60$ mas) and that the quality of reconstructed maps quality clearly exceeds Lucy-Richardson deconvolved images. With these results, the scientific analysis of the sources, according to the scientific case described in the introduction, can be addressed.

Acknowledgments

JSB acknowledges support by the “JAE-Pre” programme of the Spanish Consejo Superior de Investigaciones Científicas (CSIC). RS acknowledges support by the Ramón y Cajal programme, by grants AYA2010-17631 and AYA2009-13036 of the Spanish Ministry of Science and Innovation, and by grant P08-TIC-4075 of the Junta de Andalucía. AA acknowledges support by grant AYA2009-13036 of the Spanish Ministry of Science and Innovation and by grant P08-TIC-4075 of the Junta de Andalucía.

References

- [1] Genzel, R and Schödel, R and Ott, T and Eisenhauer, F and Hofmann, R and Lehnert, M and Eckart, A and Alexander, T and Sternberg, A and Lenzen, R and Clénet, Y and Lacombe, F and Rouan, D and Renzini, A and Tacconi-Garman, L E 2003 *ApJ* **594** 812–832
- [2] Schödel R, Eckart A, Alexander T, Merritt D, Genzel R, Sternberg A, Meyer L, Kul F, Moulataka J, Ott T and Straubmeier C 2007 *A&A* **469** 125–146
- [3] Schödel R, Ott T, Genzel R, Eckart A, Mouawad N and Alexander T 2003 *ApJ* **596** 1015–1034
- [4] Ghez A M, Becklin E, Duchjne G, Hornstein S, Morris M, Salim S and Tanner A 2003 *Astronomische Nachrichten Supplement* **324** 527–533
- [5] Krabbe A, Genzel R, Eckart A, Najarro F, Lutz D, Cameron M, Kroker H, Tacconi-Garman L E, Thatte N, Weitzel L, Drapatz S, Geballe T, Sternberg A and Kudritzki R 1995 *ApJ* **447** L95
- [6] Figer D F 2004 *The Formation and Evolution of Massive Young Star Clusters (Astronomical Society of the Pacific Conference Series vol 322)* ed H J G L M Lamers, L J Smith, & A Nota p 49
- [7] Morris M 1993 *ApJ* **408** 496–506
- [8] Paumard T, Genzel R, Martins F, Nayakshin S, Beloborodov A M, Levin Y, Trippe S, Eisenhauer F, Ott T, Gillessen S, Abuter R, Cuadra J, Alexander T and Sternberg A 2006 *ApJ* **643** 1011–1035
- [9] Bartko H, Martins F, Fritz T K, Genzel R, Levin Y, Perets H B, Paumard T, Nayakshin S, Gerhard O, Alexander T, Dodds-Eden K, Eisenhauer F, Gillessen S, Mascetti L, Ott T, Perrin G, Pfuhl O, Reid M J, Rouan D, Sternberg A and Trippe S 2009 *ApJ* **697** 1741–1763
- [10] Girard J, Pompei E, Amico P and Lidman C *Very Large Telescope NACO manual* URL <http://www.eso.org/sci/facilities/paranal/instruments/naco/doc/>
- [11] Tuthill P, Lloyd J, Ireland M, Martinache F, Monnier J, Woodruff H, ten Brummelaar T, Turner N and Townes C 2006 *Society of Photo-Optical Instrumentation Engineers (SPIE) Conference Series (Society of Photo-Optical Instrumentation Engineers (SPIE) Conference Series vol 6272)*
- [12] Diolaiti E, Bendinelli O, Bonaccini D, Close L, Currie D and Parmeggiani G 2000 *Astronomical Data Analysis Software and Systems IX (Astronomical Society of the Pacific Conference Series vol 216)* ed N Manset, C Veillet, & D Crabtree p 623
- [13] Buscher D F 1994 *Very High Angular Resolution Imaging (IAU Symposium vol 158)* ed J G Robertson & W J Tango p 91
- [14] Tanner A, Ghez A M, Morris M R and Christou J C 2005 *ApJ* **624** 742–750
- [15] Lucy L B 1974 *ApJ* **79** 745